Optimization of Tracer Dose for Scintigraphic Imagery

C. Bousnah[1] [a], S. Anebajagane[2], O. Monsarrat[2], J.-Ph. Conge[1] [b], H. Maaref[1] [c] and V. Vigneron[1] [d]

[1] *IBISC EA 4526, Univ. Evry, Université Paris-Saclay, France*
[2] *Service de Médecine Nucléaire, CHSF, Corbeil, France*

Keywords: Machine Learning, Multi-modal Imaging, Precision Medicine, Myocardial Perfusion Scintigraphy, Dose Optimization, Patient Radiation Protection.

Abstract: Myocardial scintigraphy is a non-invasive isotope examination that has played a central role in the management of these coronary heart diseases for decades.it has proven its performance in nuclear cardiology, mainly for the diagnosis of ischemia by making it possible to analyze the myocardial perfusion, and precisely, to evaluate the quality of the irrigation by the arteries and the coronaries, as well as for the diagnosis of coronary heart disease. It is based on the injection of an intravenous radioactive tracer, which, once injected, is absorbed by the heart muscle. The radiation emitted by the radioactive tracer is converted into an image by computer tomography. However, these scintigraphic images suffer from poor spatial resolution in particular, in obese patients, it is difficult to obtain images of sufficient quality using the recommended standard doses due to the attenuation of $\gamma-$rays by soft tissues (fat, fibrous tissues, etc.). This phenomenon prompts the nuclear physician to overdose the tracer and the dose of radiation received exceeds the admissible regulatory limits. In this paper we propose a machine learning model that predict the dose of tracer based on patient's morphological parameters to obtain images of sufficient quality to support the cardiovascular diagnosis while exposing him to the lowest possible doses of radiation. We show the body weight is not the best-predicting parameter for image quality.

1 INTRODUCTION

Myocardial scintigraphy has played a central role in the management of coronary heart disease for decades (Piekarski et al., 2020). Cardiovascular diseases are responsible for 17.7 million deaths worldwide each year, or 31% of deaths, causing nearly twice as many deaths as cancer (Bonow et al., 2002). The myocardiac perfusion scintigrahy (MPS) is a non-invasive nuclear medicine imaging test that uses a small amount of a radioactive tracer (usually Technetium ^{99m}Tc but also Thallium ^{201}Tl or Rubidium ^{37}Rb) to detect any difference in blood flow in the heart muscle at rest and during exercise. It is widely used to assess the extent of damage to the heart, detect myocardial structures in patients with chest pain, to look for myocardial ischemia or small atypical symptoms, etc. (Nance et al., 2014). 80,000 people per year undergo this examination in France.

[a] https://orcid.org/0000-0002-2459-8284
[b] https://orcid.org/0000-0002-8641-0312
[c] https://orcid.org/0000-0002-2459-8284
[d] https://orcid.org/0000-0001-5917-6041

The radioactive tracer ^{99m}Tc emits γ radiations detected by a $\gamma-$camera which revolves around the patient's body. Once injected, the tracer is absorbed by the heart muscle. Well-irrigated areas of the heart will emit more $\gamma-$rays than less well-irrigated areas. The images thus collected are put together to form a 3D image of the organ studied (see Fig. 1).

This assessment of myocardial perfusion can be performed at rest and / or after a myocardial ischemia challenge test (pharmacological stress or stress test). Consequently, any relative fixation deficit will be interpreted as a perfusion defect called *hypoperfusion* which may correspond to ischemia or myocardial necrosis (myocardial infarction) (Foraggi et al., 2008).

However, these scintigraphic images suffer from poor spatial resolution (a voxel $\approx$ 1 cm^3) (Patton and Turkington, 2008) and poor signal to noise ratio (SNR). In particular, in obese patients, it is difficult to obtain images of sufficient quality using the recommended standard doses due to the attenuation of $\gamma-$rays by soft tissues (fat, fibrous tissue, etc.) (Tamam et al., 2016). This phenomenon prompts the nuclear physician to *overdose* the tracer and the dose
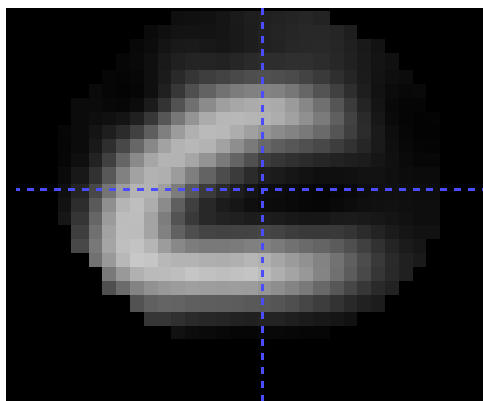
167

Figure 1: Myocardial scintigraphy image visualized with `ITKSnap`.

of radiation received exceeds the permissible regulatory limits. These limits have been specified by both the High Authority for Health (HAS) and the Nuclear Safety Authority (NSA) for the sake of radiation protection: 1 mSv per year (sum of effective doses) for the public. There are also regulatory limits for ionizing radiation for workers and staff: 20 mSv per year (sum of the effective doses). Exceeding doses may increase the risk of cancer from radiation. The recommendations of the European Association of Nuclear Medicine (EANM) specify that the dosage of the common tracer ^{99m}Tc should be calculated by the specialist only on the basis of weight. However, the attenuation of the scintigraphy images is above all influenced by the thickness of the tissues (muscle fibers, fatty tissues, bones, etc.) to be passed through, in particular in obese patients.

The dose of radio-tracer to be administered is a compromise between image quality and radiation exposure and depends on patient characteristics (*e.g.*body weight), choice of radio-pharmaceutical (^{99m}Tc or ^{201}Tl compounds), acquisition protocol (1 day or 2 days protocols, imaging time, image resolution, gated acquisition), and the type of equipment (multiple head scintillation camera or a camera based on cadmium zinc telluride (CZT) detectors). Thus, the objective of this work consists in proposing a "finer" dosage, based on the body mass index (BMI), and other morphological factors to be determined, easily identifiable by the doctors before the examination and which will allow the injection tracer to be optimally calibrated, thus limiting patient's exposure to radiation while ensuring sufficient image quality.

In the following section, we take stock of the state of the art on the assay of tracers dosage. Section 3 details the data collected for this experiment. Section 4 provides a methodology for predicting tracer dose and image quality and a discussion on the main results.

2 A SHORT REVIEW OF TRACER DOSAGE CALCULUS

Van Dijk et al. (2014) disclose a method to compensate for the decrease in image quality in obese patients by administering a patient-specific dose in myocardial perfusion imaging using a tomographie par émission monophotonique (SPECT) camera based on CZT detectors[1]. The study was carried out on 148 patients. This article proposes in particular a method for deriving a dose of tracer to be administered depending on the body-weight or scan-time protocol by calculating (Van Dijk et al., 2014):

$$d_{\text{admin}} = \frac{CW^{-b}K}{aT_{\text{scan}}}, \tag{1}$$

wherein C is the photon count, P is the body weight, K is the correction factor for the radioactive decay between the administration of tracer dose and the SPECT acquisition, T is the scanning time, a and b are adjustment parameters. The measured photon numbers were normalized based on the administered tracer dose and the scan time were correlated with body weight, body mass index to find the best predictor. From these data, a protocol to provide consistent image quality was validated in 125 new patients. Van Dijk et al. (2014) claim that weight was the main morphological parameter of the patient despite it is not a good indicator of the distribution of fat mass, especially around the heart.

(Gimelli et al., 2017) develop a software for automatic calculation of pediatric dosage of radio-pharmaceuticals, according to European Association of Nuclear Medicine (EANM) 2007 pediatric dosage card. This card is based upon the publication by Jacobs et al. (2005) who show that normalization factors for effective dose can be estimated accurately as a function of body weight W by holding only one parameter, called the 'a' value.

Dogan et al. (2019) assess the validity of automated quantitative and semi-quantitative visual analysis of total perfusion deficit using SPECT $\gamma-$camera to detect significant coronary artery disease. Zhang et al. (2015) investigate image quality, radiation dose, and diagnostic performance of prospectively ECG-triggered high-pitch coronary CT angiography at 70 kVp compared to invasive coronary angiography as reference standard. Their protocol results in an effective radiation dose of 0.2 mSv and high diagnostic accuracy for stenosis detection in a selected, non-obese population. Gould et al. (2008) compare on a total of 250 consecutive patients resting perfusion

---

[1]This camera is specially dedicated to the the heart examination.

images reconstructed using rest CT attenuation data with the same resting emission data reconstructed with post-stress CT attenuation data. No clinically significant differences were observed. And eliminating rest CT scan reduces CT radiation dose by 50%. Kero et al. (2021) suggest too that stress-first perfusion imaging (PI) using ^{99m}Tc tracer can significantly reduce the radiation dose compared with standard dose rest–stress protocols. If the stress PI results are normal (Duvall et al., 2011). Hamilton-Craig et al. (2019) examine the impact of dose reduction techniques using ECG-triggering, kVp/mAs reduction and high-pitch modes on radiation exposure in a Australian hospital. 3,000 coronary CT angiography were analyzed with mean radiation dose decreasing from 8.4 mSv to 2.8 mSv per year. Implementation of dose reduction algorithm and staff education program resulted in a 67% reduction in radiation exposure, while maintaining diagnostic specificity. Chinnaiyan et al. (2013) show that the use of newer scanner technology resulted in incremental radiation dose reduction in a statewide coronary CT angiography registry without image quality degradation.

3 MATERIALS

This experimental study is based on two recent databases which were retrieved from the nuclear physicians from Hôpital sud-francilien (CHSF).

3.1 Chest Database

The first database contains CT scans and myocardial scintigraphy images of 130 patients with cardiovascular pathology, recorded using a Siemens Symbia T2 SPECT CT γ−camera on the upper part of the patient's body (chest part). Thus, the physiological parameters of the patient and the metadata of the images (resolution, image size, image rotation, date / time, sex, age, weight, height, BMI, etc.) were recorded.

The scintigraphy images were taken in the nuclear medicine department of the CHSF, after the patient was injected with a radioactive tracer (Technetium ^{99m}Tc), which binds to the heart. Next, a NaI γ−camera[2] captures the photons emitted by the tracer and rotates around the patient's body so that the images collected are grouped together to form a 3D image of the heart (Fig. 1). Most of the examinations were carried out after a stress test that stimulates the myocardium which better absorbs the radioactive tracer (in terms of speed and homogeneity). Depend-

---

[2]Thallium-doped sodium iodide.

ing on the result of this test, another test at rest may be necessary to improve the image quality.
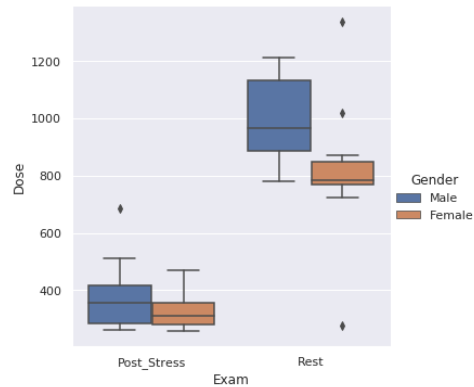

Figure 2: Boxplot of tracer dose with respect to sex and type of exam.

An `Excel` file containing information about the patient (sex, age, weight, height, BMI) was also provided with the doses used during the examination, as well as the image grade noted by the doctors before and after correction by the CT scanner. NCIQ and CIQ stand resp. for non-corrected and corrected image quality (Tab.3). The nuclear physician has in fact the possibility of improving manually with a few manipulations to improve the quality of the image in order to improve the estimation of the dosage of the tracer.

The chest database contains 58 men and 38 women aged from 43 to 93 y.o., 104 of them have done a post stress exam and 26 a rest exam. The figure 2 represents the distribution of the dose according to the examination type and to the gender. The mean dose is significantly different in the post-stress and the rest groups (Kero et al., 2021).

Table 1 summarizes the main statistics of patients.

Table 1: Chest dataset patient statistics.

variable	min	mean	max	std error
age	43	69.15	93	1.07
BMI	17	29.11	43	0.44
dose	257	478.45	1337	27.26

Most of the images before correction are of poor quality. Figure 4 shows the distribution of uncorrected image quality (IQ) by examination type (rest or post-stress). IQ stands for the image quality annotated by doctors ; it is an ordinal qualitative variable with 5 modalities $IQ_i, i = \{1,2,3,4,5\}$, IQ_1 being the highest grade to the lowest IQ_5.
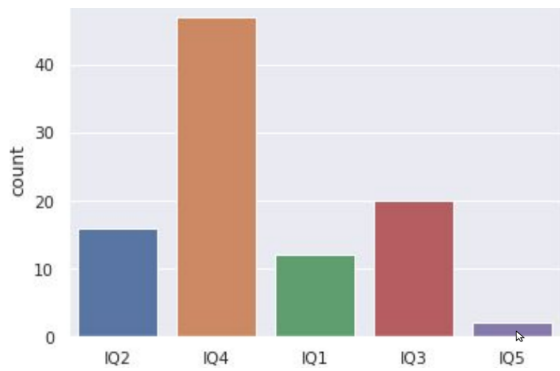
(a) non corrected image quality (NCIQ) distribution
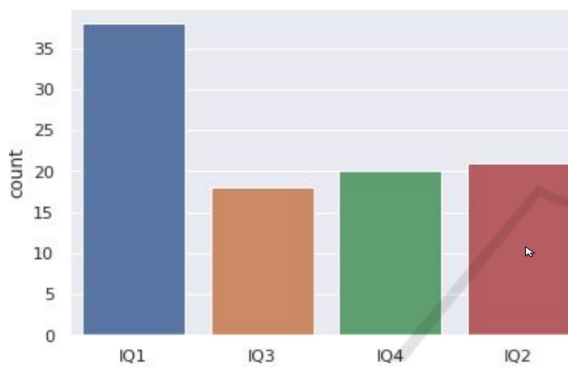
(b) corrected image quality (CIQ) distribution. After image correction, the last IQ class disapear.

Figure 3: IQ distribution. From IQ_1 (high quality) to IQ_5 (poor quality).
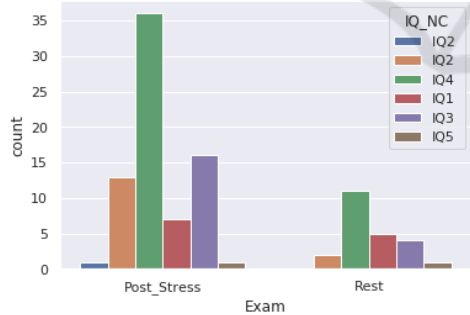

Figure 4: Distribution of image quality before correction according to the examination type.

3.2 Full-body Database

The second database contains full body scans of 247 patients acquired from examinations for other pathologies, using PET CT GE HealthCare Discovery 710 (Fig. 5). This database was used to design a model capable of predicting the abdominal perimeter which is not visible on the CT scans of the first database (see section 3.1). For example, Fig. 5 depicts a patient scan with 780 CT slices. The approxi-
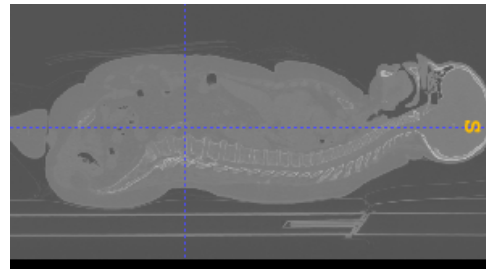

Figure 5: Full body CT scans viewed with ITKsnap.

mate intervals of the different upper body parts (thorax, diaphragm and abdomen) are determined manually using ITKsnap: thorax is located between 450-600, diaphragm between 430-460, abdomen between 200-430. The data is in DICOM format. The CT sections are 512×512 pixels, the scintigraphic images are 128×128×128. The volume of the 1st database is 12 GiB, the second 114 GiB.

4 METHODS

4.1 Calculus of Abdominal Perimeter

We propose an algorithm based on morphological factors of the patient, easily identifiable by doctors *before* the examination, which makes it possible to optimize the quantity of radioactive tracer while ensuring the good image quality.

The proposed morphological factors are: *(a)* sex *(b)* age *(c)* body mass index (the weight/height^2 ratio) *(d)* thoracic perimeter *(e)* abdominal perimeter. The parameters (a-c) are provided by doctors in the patient's medical record. The thoracic and abdominal perimeters are not measured in the clinical practice; one of the objectives of this work is to decide if these parameters are relevant for the choice of the optimal dose. To extract these two perimeters from the CT scans, we had to segment the region of interest, so that we keep the part of the body and we eliminate the chassis. For this, we used a hysteresis thresholding, followed by a morphological opening, *i.e.* an erosion followed by a dilation (Serra, 1983).

In the hysteresis thresholding technique, the high threshold represents the most significant pixels of the image which, in our case, correspond to the rib cage bones (Fig. 6). The lower threshold highlights the weaker pixels that are connected with the stronger ones. The threshold values are determined by trial and error.

After the hysteresis thresholding, some noise remains on some images (see Fig. 7a). To clean it, we
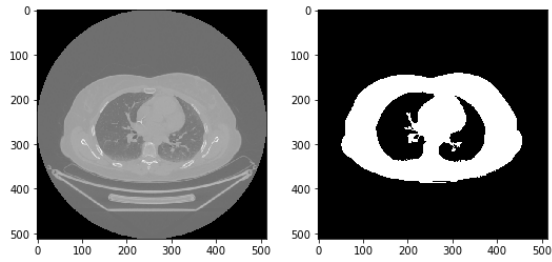
(a) Visualization of a CT (b) Hysteresis thresholding. slice.

Figure 6: Thoracic scan segmentation using `Pydicom`, a Python package for working with DICOM files.

used morphological filtering named *opening*. Next, we determined the convex hull of the segmented region, because the thoracic perimeter does not exactly follow the shape of the rib cage (Fig. 7b). Finally, we calculated the convex perimeter that we recorded in a `csv` file. This operation is repeated automatically for all scans for each patient.
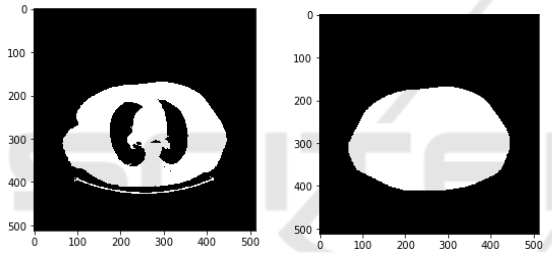

(a) Hysteresis threshold   (b) Convex hull

Figure 7: Extraction of the perimeter.

For CT scans that only contain the thoracic part of the body, the maximum of the calculated perimeters is considered the thoracic perimeter. Since those scans do not include the patient's abdominal part, we set up a training model that predicts the abdominal perimeter from the chest perimeter using whole body images (Fig. 5). First, the entire body perimeters from the CT scans are extracted for each patient as depicted in Fig. 8a, producing the graph $\mathcal{C}$ in function of the slide number k.

Here comes a first difficulty: the number of each patient's slices is proportional to the patient's height which makes it difficult to localize exactly the thorax dimension. The total number of slides varies between 705 and 1120 on the whole data set. In the figure 5 for example, 780 CT slices define the patient upper body. `ITKsnap` is used to determine automatically the thoracic and abdomen part the interval I_T, respectively I_A, occupied by the thorax, resp. the abdomen, as in Figures 8a and 8b. I_T and I_A are delimited with bullet points corresponding to the inflection points in
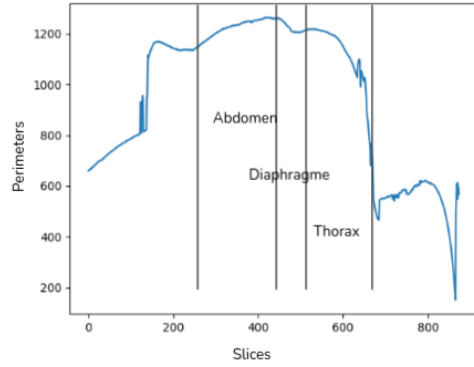
(a) Raw graph obtained from the perimeters of the convex hull of the CT slices.
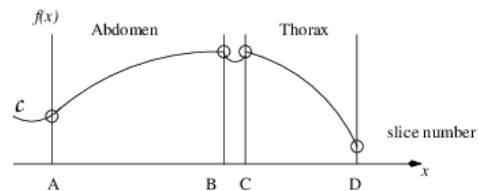
(b) Approximate form of the graph 8a. The intervals are delimited with bullets that correspond to curvature change points in the graph.

Figure 8: Graph of the upper-body perimeters.

$\mathcal{C}$. Consider that the function $f(x)$ of graph $\mathcal{C}$ is locally 2 times continuously differentiable. The inflection points are those where the second derivative vanishes by changing of sign, *i.e.* $\frac{\partial^2 f}{\partial x^2} = 0$. The same procedure is applied to all the patients. The approximate intervals of the different parts are $I_T = [450 : 600]$ for the thorax and $I_A = [200 : 430]$ for the abdomen.

The second step consists in developing a learning model that predicts the abdominal perimeter from the thoracic perimeter, sex, age, size and BMI (see Fig. 11). So, we separate the database into 3 subbases: learning, validation and test bases representing resp. 65%, 15% and 20% of the samples. For more details on neural networks, refer to Bishop (2006). The table 2 summarizes the characteristics of the proposed neural network.

Table 2: Neural network's architecture to predict abdominal perimeter.

Inputs	thoracic perimeter P_{Th}, sex, age, height, BMI
hidden neurons	10
activation function	ReLU
optimizer	Adam
Loss	MSE
Batch	7
Epoch	250
Output	abdominal perimeter P_{Abd}

The learning and validation loss decreases to stability as shown in the figure 9.
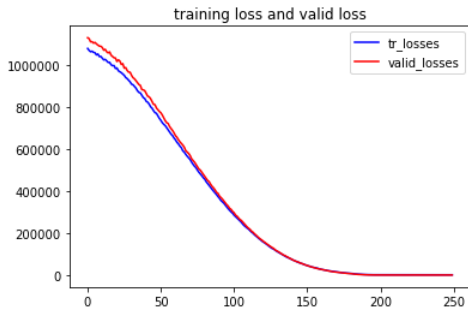

Figure 9: Learning and validation losses.

To evaluate the model accuracy, we used the coefficient of determination R-square defined, for univariate series as follows :

$$R^2 = \frac{\sum_{i=1}^{N}(\hat{Y}_i - \bar{Y})^2}{\sum_{i=1}^{N}(Y_i - \bar{Y})^2} = 1 - \frac{\sum_{i=1}^{N}(Y_i - \hat{Y}_i)^2}{\sum_{i=1}^{N}(Y_i - \bar{Y})^2}, \quad (2)$$

where $Y_i, \hat{Y}_i, \bar{Y}$ are, for this model, resp. the estimated, expected and mean abdominal perimeters. The model performances were evaluated on the test dataset. The R^2 is 83%, and Pearson's product-moment correlation coefficient (or Pearson correlation coefficient, for short) which measure of the strength of a linear association between predicted and expected abdominal perimeters, resp. $\hat{P}_{\text{Abd}}$ and P_{Abd}^* is 91.11%.
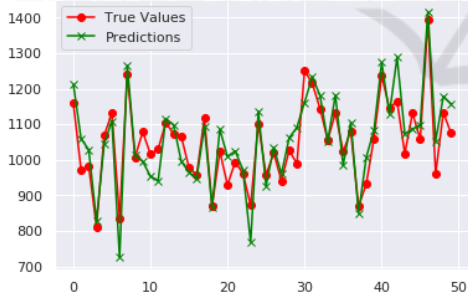

Figure 10: Perimeter values predicted by neural network regression / real values (50 patients).

4.2 Optimization of the Amount of Administered Radiotracer Dosage

Unlike conventional guidelines suggesting considerably large dosage levels for obese patients (Karakatsanis et al., 2015), the objective of this study is to moderate dosage for obese patients and dosage reduction for slimmer patients which are usually based on the *only patient weight*. In this section the relevance of the abdominal perimeter for optimizing tracer dose is

evaluated. The proposed model is designed to help doctors to choose the best dose / image quality response model. We propose utilizing a neural network model to predict the radioactive tracer dose according to the type of examination performed (post stress or at rest), and according to the IQ, *i.e.*NCIQ versus CIQ, plus other morphological parameters (age, weight, height, BMI, abdominal perimeter). However, the limited understanding of which physiological model is the least biased for the prediction of radiotracer dosage increases attrition in the decision-making process. There are several possible causes for the inconsistencies between predictive and empirical dosage: patient obesity, differences in metabolic rates for the same radiotracer, routine practice, equipment technical evolutions, etc.

Differences in metabolism and anatomical barriers can be challenging to predict and minimize. Notwithstanding, it is possible to improve predictive dosage models if the known inaccuracies result from systematically modeling over- or underestimations, rather than unpredictable spurious causes.
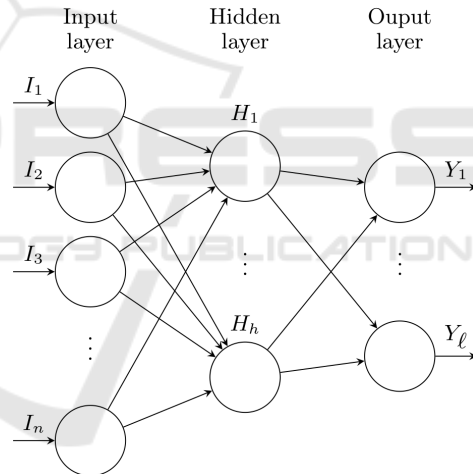
Figure 11: A shallow network with d inputs, h hidden neurons and ℓ outputs.

Table 3 summarizes the characteristics of the proposed neural network. The `Adam` optimizer is used for training the network with a learning rate equal to 0.001.

We were careful not to include the weight in the dependent variables (inputs) in Tab. 3 since, in the database, the doses of tracer were calculated by the doctors from the weight. Obviously using BMI or weight in our model would have biased the results, so they were deliberately omitted.

To measure the relevance of each parameter for dose prediction, we tested different combinations of inputs among which age, P_{Th}, P_{Abd}, sex, type of examination (post-stress versus rest).

Table 3: Neural network's architecture to predict tracer dose.

Inputs	thoracic abdominal P_{Abd}, sex, age, height
hidden neurons	12
activation function	ReLU
Optimiser	Adam
Loss	MSELoss
Batch	7
Epoch	12,500
Output	Dose

After 12,500 epochs of training, the estimator network converges; the learning and validation losses decrease to stability as shown in the figure 12.

(a) Corrected images.

(b) Non corrected images.

Figure 12: Learning curves of dose prediction model with corrected images and uncorrected images.

The model was evaluated on never-before-seen data from the test base which contains (only) 14 patients due to the short size of the database. The figure 13 represents the dose values predicted by the neural network versus to the real values for corrected images and for non corrected images.

It is possible to stratify the administered dose by the type of examination status because the latter is suspected to account for the response variable. The summary statistics are discernably different than they would be for unstratified data. A between groups z-test is used to compare the results in the rest and post-stress groups. The null hypothesis with the between

groups z-test is that the R^2 scores in the two groups are equal in the population $p_1 = p_2$ where p_1 and p_2 are the R^2 scores for the two groups. z-value is the ratio:

$$z = \frac{p_1 - p_2}{\text{se}}, \quad (3)$$

where 'se' represents the sampling variability, p_{12} the pooled sample R^2 score:

$$p_{12} = \frac{n_1 p_1 + n_2 p_2}{n_1 + n_2}, \quad (4)$$

with $n_1 = 36$ and $n_2 = 94$ the sample sizes for each of the two groups. The standard error of the sampling distribution difference between the two proportions is:

$$\text{se} = p_{12}(1 - p_{12})\sqrt{\frac{1}{n_1} + \frac{1}{n_2}}. \quad (5)$$

The null hypothesis was rejected with a p-value of 0.0028 assessing the prediction dose is better predicted in the post-stress group than in the rest group.

The R^2 scores given in Tab. 4 and calculated from Eq. (4), merge the response variables of the strata/groups. Thoracic or abdominal perimeters combined with age or the type of examination give very good scores. Combining all morphological parameters as inputs gives R^2 scores of **91,56%** with corrected image quality, and 89,81% with non corrected image quality.

Table 4: Predicted R^2 scores for some combinations of inputs of corrected images.

| Inputs	R^2 score
BMI, type_exam	90,33%
P_{Th}, type_exam	88,35%
P_{Abd}, type_exam	87,39%
age, P_{Th}, type_exam	**91,56%**
age, sex, P_{Th}, type_exam	89,14%
age, P_{Abd}, type_exam	90,82%

Table 5 gives the scores obtained for some combinations of input parameters in the case of corrected images and non corrected ones.

Table 5: Predicted R^2 scores for corrected/uncorrected images.

	Inputs	R^2 score
corrected image	age, P_{Th}, type_exam	**92,42%**
	age, type_exam	**92,16%**
uncorrected image	age, P_{Th}, type_exam	90,73 %
	age, type_exam	90,71 %

4.3 Prediction of the Image Grade from the Tracer Dose

Finally, a last study is presented in this section, *i.e.* a new model capable to predict the image quality based
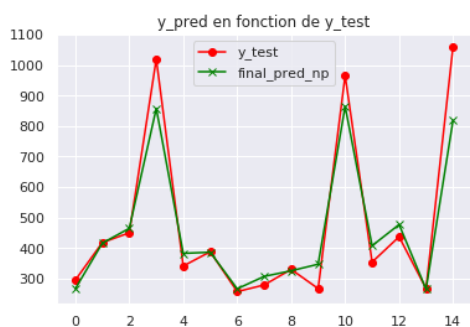
(a) Results for corrected images.
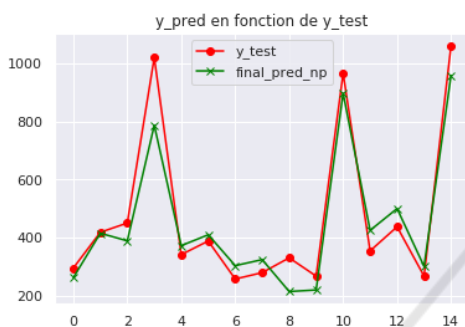
(b) Results for non corrected images.

Figure 13: Predicted radiotracer dose by the neural network model versus expected values (14 patients).

Table 6: Overall performance of the neural classifier.

Class	P	R
IQ_1	0.945	0.777
IQ_2	0.562	0.900
IQ_3	0.833	0.666
IQ_4	0.793	0.920
IQ_i	0.166	0.200

4.4 Discussion

Decreasing image quality in heavier patients can be compensated by administration of a patient-specific dose in myocardial perfusion imaging using a cadmium zinc telluride-based SPECT camera. From collected data, a protocol to provide optimal image quality was derived, and subsequently validated in 250 patients. Thoracic and abdominal perimeters are found to be best predicting parameters for image quality. These results pave the way to patient-specific protocol resulting in an image quality less depending on patient's weight.

5 CONCLUSIONS

The calculation of the effective radiotracer dose for a myocardial perfusion scintigraphy based on the known anatomical parameters of the patient is novel. The prediction results could be further improved by training on a larger database. The relevance of the thoracic and abdominal perimeters has been proven, so they can also be used as dose predictors, especially in obese patients whose BMI does not really represent the distribution of fat around the heart. The body weight may be not the best-predicting parameter for image quality.

on age, P_{Th}, P_{Abd}, sex, type of examination.

It is typically a multi-class problem ith N=130 observations and $K = 5$ classes $IQ_i, i = 1, \ldots, 5$. Classifier performance is typically defined according to the confusion matrix associated with the classifier. Based on the entries of the matrix, it is possible to compute sensitivity (recall), specificity, and precision. In the following we will use TP_i, FP_i and FN_i to resp. indicate true positives, false positives, and false negatives in the confusion matrix associated with the i-th class. Precision and recall are indicated resp. by P and recall by R.

A confusion matrix for every class $C_i, i \in \{1, \ldots, 5\}$ is computed such that the i-th confusion matrix considers class C_i as the positive class and all other classes C_j with $j \neq i$ as the negative class. Each confusion matrix pools all observations labeled with a class other than C_i as the negative class. Table 6 summarizes the performances across all classes. These data indicate that, overall, performance is quite high. However, our hypothetical classifier underperforms for individual classes such as class IQ_2 (precision) and class IQ_5 (both precision and recall).

REFERENCES

Bishop, C. M. (2006). *Pattern Recognition and Machine Learning (Information Science and Statistics)*. Springer-Verlag, Berlin, Heidelberg.

Bonow, R., Smaha, L., Smith, S., Mensah, G., and Lenfant, C. (2002). World heart day 2002: The international burden of cardiovascular disease: Responding to the emerging global epidemic. *Circulation*, 106:1602–5.

Chinnaiyan, K., Boura, J., Depetris, A., Gentry, R., Abidov, A., Share, D., and Raff, G. (2013). Progressive radiation dose reduction from coronary computed tomography angiography in a statewide collaborative quality improvement program: Results from the advanced cardiovascular imaging consortium (ACIC). *Circulation. Cardiovascular imaging*, 6.

Dogan, C., Cinaral, S. F., Karag oz, A., Bayram, Z., onal, C., Candan, O., Acar, R., Cap, M., Erdogan, E., Hakgor, A., Akbal, O., Uslu, A., Kaymaz, C., and Ozdemir, N. (2019). Comparison of automated quantification and semiquantitative visual analysis findings of iq spect mpi with conventional coronary angiography in patients with stable angina. *Turk Kardiyoloji Derneginin yayin organidir*.

Duvall, W., Croft, L., Ginsberg, E., Einstein, A., Guma, K., and Henzlova, T. (2011). The accurate determination of college students' coefficients of friction. *J Nucl Cardio*, 18(2):847—–857.

Foraggi, M., Pierquet-Ghazzar, N., and Maunoury, C. (2008). Detection de l'ischemie myocardique en scintigraphie. *Journal de Radiologie*, 89(10):1283.

Gimelli, A., Achenbach, S., Buechel, R. R., Edvardsen, T., Francone, M., Gaemperli, O., Hacker, M., Hyafil, F., Kaufmann, P. A., Lancellotti, P., Nieman, K., Pontone, G., Pugliese, F., Verberne, H. J., Gutberlet, M., Bax, J. J., Neglia, D., and Committee, . E. S. D. (2017). Strategies for radiation dose reduction in nuclear cardiology and cardiac computed tomography imaging: a report from the European Association of Cardiovascular Imaging (EACVI), the Cardiovascular Committee of European Association of Nuclear Medicine (EANM), and the European Society of Cardiovascular Radiology (ESCR). *European Heart Journal*, 39(4):286–296.

Gould, K. L., Pan, T., Loghin, C., Johnson, N. P., and Sdringola, S. (2008). Reducing radiation dose in rest–stress cardiac pet/ct by single poststress cine ct for attenuation correction: Quantitative validation. *Journal of Nuclear Medicine*, 49(5):738–745.

Hamilton-Craig, C., Tandon, K., Kwan, B., DeBoni, K., Burley, C., Wesley, A., O'Rourke, R., Neill, J., and Branch, K. (2019). Coronary ct radiation dose reduction strategies at an australian tertiary care center - improvements in radiation exposure through an evidence-based approach. *Journal of Medical Radiation Sciences*, 67.

Jacobs, F., Thierens, H., Piepsz, A., Bacher, K., Wiele, C., Ham, H., and Dierckx, R. (2005). Optimised tracer-dependent dosage cards to obtain weight-independent effective doses. *European journal of nuclear medicine and molecular imaging*, 32:581–8.

Karakatsanis, N., Fokou, E., and Tsoumpas, C. (2015). Dosage optimization in positron emission tomography: state-of-the-art methods and future prospects. *Am J Nucl Med Mol Imaging*, 5(5):527–547.

Kero, T., Saraste, A., Lagerqvist, B., S orensen, J., Pikkarainen, E., Lubberink, M., and Knuuti, J. (2021). Quantitative myocardial perfusion response to adenosine and regadenoson in patients with suspected coronary artery disease. *Journal of nuclear cardiology*.

Nance, J., Schoepf, U., Bamberg, F., Ruzsics, B., Vliegenthart, R., and Bastarrika, G., editors (2014). *CT Imaging of Myocardial Perfusion and Viability: Beyond Structure and Function*. Medical Radiology - Diagnostic Imaging. Springer-Verlag, Berlin Heidelberg.

Patton, J. and Turkington, T. (2008). Spect/ct physical principles and attenuation correction. *J Nucl Med Technol*, 36(1):1–10.

Piekarski, E., Manrique, A., Rouzet, F., and Le Guludec, D. (2020). Current status of myocardial perfusion imaging with new spect/ct cameras. *Seminars in Nuclear Medicine*, 50(3):219 – 226. Developments in Cardiac Imaging, part 1.

Serra, J. (1983). *Image Analysis and Mathematical Morphology*. Academic Press, Inc., USA.

Tamam, M., Mulazimoglu, M., Edis, N., and Ozpacaci, T. (2016). The value of attenuation correction in hybrid cardiac spect/ct on inferior wall according to body mass index. *J Nucl Med*, 15(1):18–23.

Van Dijk, J., Jager, P., Mouden, M., Slump, C., Ottervanger, J., de Boer, J., Oostdijk, A., and van Dalen, J. (2014). Development and validation of a patient-tailored dose regime in myocardial perfusion imaging using czt-spect. *Journal of nuclear cardiology*, 21.

Zhang, L., Wang, Y., Schoepf, U., Meinel, F., Bayer, R., Qi, L., Cao, J., Zhou, C., Zhao, Y., Li, X., Gong, J., Jin, Z., and Lu, G. (2015). Image quality, radiation dose, and diagnostic accuracy of prospectively ecg-triggered high-pitch coronary ct angiography at 70 kvp in a clinical setting: comparison with invasive coronary angiography. *European radiology*, 26.